A chemical kinetics simulation of plasma-catalytic dry reforming

Shengfei Wang, Vandad-Julien Rohani, Paul Dupont, Sylvain Pagnon, Laurent Fulcheri

A chemical kinetics simulation of plasma-catalytic dry reforming

Shengfei Wang *, Vandad Rohani *, Paul Dupont, Sylvain Pagnon, Laurent Fulcheri

Mines Paris, PSL University, Centre Procédés Energies Renouvelables et Systèmes Energétiques (PERSEE), 06904 Sophia Antipolis, France

*Corresponding author

Shengfei Wang: shengfei.wang@minesparis.psl.eu

Vandad Rohani: vandad-julien.rohani@minesparis.psl.eu

Abstract

The recent intensification of the research on plasma-catalytic dry reforming as a promising route in synthesis chemistry makes us understand more its underlying mechanisms. A comprehensive zero-dimension kinetic model is proposed in which homogeneous reactions as well as heterogeneous reactions are considered together. The evolution of the species densities is followed in time and the reaction routes are analyzed. An insight of products formation is given. As an example of application, the model allows to predict a decrease of 22.45% and 17.05% on the apparent activation energies of CO_2 and CH_4 respectively when Rh-based catalysts are used with plasma.

Keywords: Plasma-catalysis; Dry reforming; Chemical kinetics; Reaction mechanism; Activation energy

1. Introduction

Nowadays, plasma-catalytic dry reforming (DRM) is considered a promising process for electrically converting the two main greenhouses gases, i.e. carbon dioxide and methane, into syngas. Compared with traditional way, plasma-catalysis initiates the reactions with a lower energy consumption by generating an exclusive non-equilibrium environment which contains many active species around the catalyst at low gas temperature [1,2]. In such non-thermal plasma, the electron temperature is much higher than the gas temperature allowing to trigger reactions while limiting the dissipation by relaxation, opening the way of higher energy efficiency conversion. At current research stage, plasma-catalytic DRM has been wildly investigated. The main products of this process are syngas, gaseous hydrocarbons and liquid oxygenates [3,4]. Unfortunately, due to the complexity of plasma, the insight of reaction mechanism and kinetic still remain a great challenge so far.

Currently, experimental attempts have been conducted in order to determine the nature of the plasma-catalytic interaction. Microscopic processes have been partially described somehow by using state-of-art characterization methods, such as in-situ Diffuse Reflectance Infrared Fourier Transform spectroscopy (DRIFT) and Optical Emission Spectroscopy (OES) [5–7]. The kinetics and reaction mechanisms of plasma-catalysis are described and explained to a certain extent. However, this is not enough for a comprehensive understanding of the overall process, some basic questions remain unanswered.

In parallel, numerical modelling provides an approach to describe nonthermal plasma (NTP) from a theoretical point of view. Bogaerts et al., [8–12] performed a systematic study on the simulations of plasma process (such as CO_2 splitting, dry reforming and CH_4 partial oxidation). Robby et al., evaluated the chemical reactions, which involve the vibrational states of CO_2, O_2, and CO, in plasma assisted splitting of CO_2 by using a zero-dimensional (0D) kinetics modelling [13]. They found the contribution of vibrationally excited CO_2 levels in the splitting is significant while it would be even higher if the inter-pulse time is short enough due to the accumulation effects. Ramses et al., conducted a computational study for the dry reforming of methane in a dielectric barrier discharge plasma reactor. Their calculations illustrated the chemical pathways of the

conversion in detail and compared the selectivity of the products on the real residence time scale by assuming a large number of consecutive micro-discharge pulses [11].

The interactions between plasma species and catalyst surface (adsorption behavior) caught more and more attention recently since it is an essential part of plasma-catalysis by affecting surface reactions (e.g. Eley-Rideal reactions). Various chemical kinetics modelling researches have been reported [14–18]. For the nitrogen fixation, such as nitrogen oxidation and ammonia synthesis, well-established mechanism in non-thermal plasma and on transition metals are coupled to predict the chemical product formation. Schneider et al., [16] reported that plasma excited species enhanced turnover frequencies of both Pt and Au. By comparing NO production over plasma/Pt and plasma/Au, the modelling theoretically indicated that plasma-catalyst combinations should consider the properties of plasma, material and the coupling of them. The simulation also predicts that metals binding nitrogen more weakly have smaller hydrogenation barriers [17]. On these optimal catalysts, the rate enhancements are, consequently, higher for these metals.

Inevitably, some details of active plasma species and plasma processes are necessarily neglected for more complicated processes, such as DRM, Partial Oxidation of Methane (POM) and CO_2 hydrogenation. In those processes, more reactions are involved in the formation of syngas, hydrocarbons and oxygenates. As a consequence, the simulation currently is more concerned with a certain aspect in plasma-catalysis, for instance, the role of plasma species, nonoxidative coupling reactions, and etc. A simple microkinetic model for C-C coupling over a transition metal surface was built for nonoxidative coupling of methane. The modelling predicts that vibrationally excited methane and presence of catalyst lead to the increase of ethylene formation [19,20]. By building microkinetic model on Pt (111) surface, Loenders et al., [21] investigated the effects of three Eley-Rideal reactions and find that radicals govern the surface chemistry for the plasma-catalytic POM. They also pointed out that, currently, the lack of activation energies of extended chemistry set is limiting the understanding of Eley-Rideal reactions. Radicals and Eley-Rideal reactions also play an important role in catalytic hydrogenation of CO_2 to CH_3OH. Over a Cu (111) facet, increased H* coverage results in the higher production through the formate path via HCOOH* which consequently leads to the higher CH_3OH production in plasma-catalysis [22]. Shao et al., [23] reported that CH_3OH(s) could also be produced by the Eley-Rideal reaction in which intermediate

$CH_3O(s)$ reacts with H. Similarly, relevant kinetic data on the reactions and rate coefficients are not clear to construct a comprehensive model.

Nevertheless, kinetic study of plasma process on a macroscopic scale is still insufficient considering its unique and complex characteristics. It is worth noting that most of the fundamental researches focus on the micro-reactions on a certain facet of metal catalysts, such as Pt (111), Ni (111), Cu (100) and etc [15,18–22]. Obviously, regarding the industrial catalytic applications, such a description is not perfect. However, it is impractical to have a perfect and accurate understanding of the processes in plasma-catalysis due to the limitations of current research. In addition to the microscopic surface of the catalyst, macroscopically, the internal characteristics of the reactor, fluid flow, heat and mass transfer, chemical reactions, and reduced electric field in the reactor also greatly affect the catalytic process.

In practice, apparent activation energy plays an important role in the field of chemical kinetics while it is still very difficult to calculate in plasma-catalysis. Hicks et al., [24] constructed a modified Arrhenius equation which plot the plasma reaction rate constants and the reciprocal of the DBD plasma power. Due to the complicated discharged environment, the energy barrier is found to decrease in plasma-assisted catalysis. Besides, surface reaction dynamics on the catalytic surface can unavoidably influence the physical properties and chemical reactions. Unfortunately, few of relevant studies elucidated the plasma kinetics in detail experimentally or theoretically. It is crucial for developing a universal method to calculate apparent activation energy theoretically. Establishing a general model suitable for process simulation of industrial catalysis for the future is rather meaningful. Instead of focusing on specific reactions on certain facet, this general model may also be used as an input chemical set for Computational Fluid Dynamics (CFD) simulations (e.g. Ansys Fluent) which could be used to gain insight into interaction of plasma and catalysts.

The goal of this work is to focus on the plasma chemistry during the power pulse and its afterglow from a numerical point of view. We propose an approach to understand micro kinetic mechanism for plasma-assisted dry reforming process which also has potential to be further applied in fluid simulations and industrial process simulations. In this study, we simulated a 0D-plasma reactor by using two softwares: BOLSIG+ and CHEMKIN. The electron temperature, number density and production rate of key intermediates and products are first calculated. Subsequently, critical

reaction channels, including electron-impacted reactions, neutral reactions, ion reactions and etc., are investigated to describe the reaction mechanisms on a micro time scale. Additionally, we also investigate the role of catalysts by inducing the surface reaction mechanism into the model. We manage to compare the effect of surface reactions and calculate the apparent activation energy via a numerical route.

2. Description of the methodology

2.1 Species

We established a 0D kinetic model in which the species and density distribution are not considered and then, it is solved by CHEMKIN. The kinetic model contains 19 molecules, 38 charged species, 29 radicals, and electrons which are listed in Table 1. Those particles collide with each other and generate a large amount of elementary reactions correspondingly. Based on the plasma chemistry developed by De Bie, Zheng, Tosi and et al., [9,25,26] we summarize 868 elementary reactions, including electron impact reactions, electron-ion recombination reactions, ion-neutral reactions, ion-ion reactions and neutral–neutral reactions, in our simulation work of plasma-catalysis.

Table 1. Summary of species included in the modelling.

Molecules	Radicals	Positive species	Negative species
CO_2 CO H_2 O_2	C_2O H O OH	CO_2^+ CO^+ H_2^+ H_3^+	
H_2O H_2O_2 CH_4	HO_2 O_2H C CH	OH^+ H_3O^+ H_2O^+ O_2^+	
C_2H_2 C_2H_4	CH_2 CH_3 C_2 C_2H	O^+ H^+ CH_5^+ CH_4^+	O_2^- O^- H^-
C_2H_6 C_3H_6 C_3H_8	C_2H_3 C_2H_5 C_3H_7	CH_3^+ CH_2^+ CH^+ O_2H^+	OH^- CH_2^-
CH_3OH HCOOH	HCO CH_2O	$C_2H_6^+$ $C_2H_5^+$ $C_2H_4^+$	Electrons
CH_3CHO	CH_2OH CH_3O	$C_2H_3^+$ $C_2H_2^+$ C_2H^+ C_2^+	
CH_3COOH	COOH CH_2CO	C^+ HCO^+ CH_2O^+	
C_2H_5OH C_3H_7OH	CH_3CO C_2HO	CH_3O^+ $HCOOH^+$	

C_2H_5COOH	CH_2CHO	C_2H_5CO	$C_2H_5OH^+$	$CHCO^+$
C_3H_7COOH	C_3H_7CO	C_2H_5O	CH_2CO^+	CH_3CO^+ HCO_2^+

2.2 Kinetic model

To begin with, the 0D kinetic model is first used by ignoring the configuration of plasma reactor and the effects of catalysts (as shown in Fig. 1). Several simplifying assumptions are made in the model. The rate of conversion of reactants to products is controlled by chemical reaction rates and not by mixing processes. Mass transport to the reactor walls is assumed to be infinitely fast. Natural convection and heat transfer in the reactor are ignored.

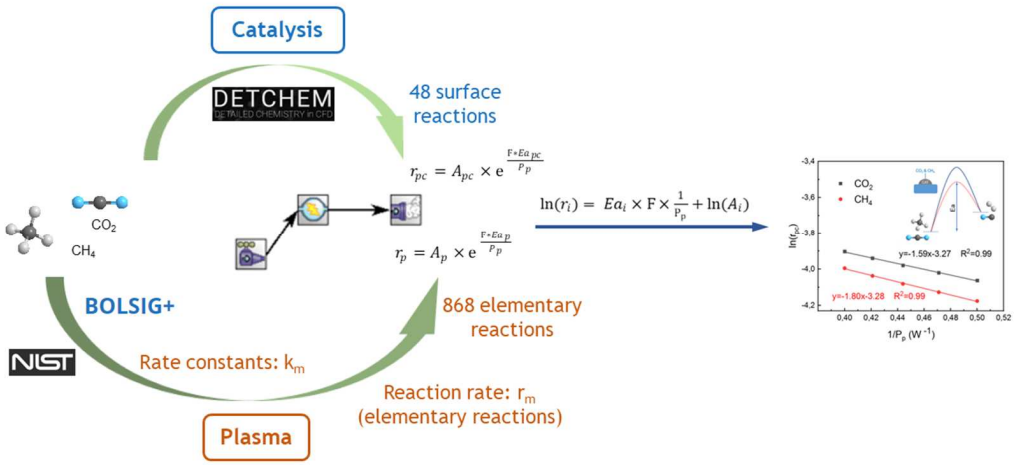

Fig. 1. Diagram of modelling.

In this model, stable molecules are first initiated by energetic electrons, creating excited particles, positive and negative ions, accompanied by the electron-ion recombination reactions in plasma environment which are also meaningful for the formation of the intermediates. In the gas phase, various products are formed from active intermediates via electron-neutral, electron-ion, ion-ion, ion-neutral and neutral-neutral reactions. For a general elementary reaction in proposed mechanism:

$$A_m + B_m \leftrightarrow C_m + D_m \quad (1)$$

The reaction rate of species A for the m^{th} reaction is defined as $r_m = d[A_m]/dt$.

$$r_m = \frac{-d[A_m]}{dt} = k_m[A_m][B_m] \ (m = 1, 2, 3, \ldots \ldots M) \quad (2)$$

The rate constants for the m^{th} reaction are expressed as k_m and the concentrations of reactants are written as $[A_m]$ and $[B_m]$.

$$k_m = a_m \left(\frac{T}{298}\right)^{\beta} \exp\left(-\frac{E_{am}}{RT}\right) \ (m = 1, 2, 3, \ldots \ldots M) \quad (3)$$

Where a_m is the preexponential factor which is a temperature-independent constant, T is refers to the electron temperature or gas temperature in electron-impact reaction or other reaction respectively, E_{am} is the activation energy for the m^{th} reaction. Consequently, the reaction rates of the nth species (r_n) are defined as:

$$r_n = \sum_{m=1}^{M} r_m {\alpha_{nm}}^f - \sum_{m=1}^{M} r_m {\alpha_{nm}}^c, (n = 1, 2, 3, \ldots \ldots N) \quad (4)$$

Where the symbols of α_{nm}^f represent n^{th} species' stoichiometric coefficient in the m^{th} formation reaction, while α_{nm}^c represent its stoichiometric coefficient in the m^{th} consumption reaction.

Based on the electron collision cross-section from the online LXcat database, the rate coefficient of electron impact reaction is obtained as a function of the electron temperature. The relationship between them is established by the following energy balance equation [25]:

$$\frac{d}{d_t}\left(\frac{3}{2} n_e k_B T_e\right) = Q_{sou} - Q_{els} - Q_{ine} \quad (5)$$

Where, in the term at the left-hand side of this equation, n_e is the electron density, k_B is Boltzmann's constant, T_e is the electron temperature. At the right-hand side of this equation, the first term represents the energy gain due to Joule heating which is an input of the model. It can be chosen under the form of a time dependent function $Q_{sou}(t)$, as we will see in section 3. The second and third terms denote the energy loss due to elastic and inelastic collisions, respectively.

$$Q_{els} = \sum \frac{3}{2} n_e \nu_{mi} \left(\frac{2m_e}{M_i}\right) k_B (T_e - T_i) \quad (6)$$

$$Q_{ine} = \sum n_e \, k_l N_l \Delta\varepsilon_l \quad (7)$$

In the equation of elastic collisions, T_i and M_i are the temperature and mass of species i, m_e is the electron mass, ν_{mi} is the electron momentum transfer collision frequency with species i. In the equation of inelastic collisions, N_l is the density of the gas phase collision partner, k_l is the reaction rate coefficient for the l^{th} electron impact process and $\Delta\varepsilon_i$ is the corresponding change in the electron energy.

Thus, we first use BOLSIG+ for solution of the above equation in order to obtain the rate coefficients of the electron-impact reactions. Then, Arrhenius coefficients (for CHENKIN input data) are obtained by curve fitting since rate coefficients are assumed to be a function of the mean electron energy [25]. Besides the electron impacted reaction, the reactions involving ions, radicals and molecules contribute greatly to the plasma chemistry and pulses. The Arrhenius rate coefficients and activation energy of the radical reactions are obtained from NIST Chemistry WebBook while the kinetic parameters are acquired from the UMIST Database for the ion involved reactions [27,28].

2.3 Calculation of apparent activation energy

According to the method presented in the literature [24,29], apparent activation barrier (E_a, kJ mol^{-1}) of the NTP-catalysis was obtained by using a modified Arrhenius law:

$$r_p = A_p \times \mathrm{e}^{\frac{F*Ea_p}{P_p}} \quad (8)$$

where r_p is the reaction rate of plasma assisted dry reforming, A_p is Arrhenius rate coefficients, F is the total flow rate of feed gas (50 mL min^{-1}), while P_p is the plasma power (W). In this work, the conversion rate of CO_2 and CH_4 are calculated by using a plasma Perfectly Stirred Reactor (PSR) reactor and the DBD discharge power is fixed between 2 and 3 W. The apparent activation energy of plasma-catalytic dry reforming was also obtained by using a modified Arrhenius law:

$$r_{pc} = A_{pc} \times \mathrm{e}^{\frac{F*Ea_{pc}}{P_p}} \quad (9)$$

Now, what we aimed to see were the differences between A_p and A_{pc} from one side, and Ea_p and Ea_{pc} from another side.

For both plasma-catalysis, ln (r_i) and the inverse of plasma power ($1/P_p$) are plotted, then the slopes are obtained by linear fitting of them according to:

$$\ln(r_i) = Ea_i \times \mathrm{F} \times \frac{1}{\mathrm{P_p}} + \ln(A_i) \quad (10)$$

We neglected the contribution of thermal-catalytic processes since gas temperature in this model is fixed to 300K,

2.4 Surface mechanism

We also consider the surface reaction kinetics (Table S3 in Supporting Information.) in which the rate constants of adsorption, desorption and surface reactions are presented in our model. The surface reaction mechanism consists of 13 surface species and 42 surface reactions [30]. The surface site density of the catalyst is 2.66×10^{-9} mol/cm^2 [31]. The reactants firstly adsorb on the catalyst surface:

$CO_2 + Rh(s) \rightarrow CO_2(s)$ (RS-04)

$CH_4 + Rh(s) \rightarrow CH_4(s)$ (RS-06)

The activation processes of CO_2 and CH_4 occur stepwise on the Rh sites after the adsorption:

$CO_2(s) + Rh(s) \rightarrow CO(s) + O(s)$ (RS-22)

$CH_4(s) + Rh(s) \rightarrow CH_3(s) + H(s)$ (RS-33)

Dissociated with other adsorbed species:

$CH_4(s) + O(s) \rightarrow CH_3(s) + OH(s)$ (RS-41)

and desorption of products and reactants:

$H(s) + H(s) \rightarrow H_2 + Rh(s)$ (RS-07)

$CO_2(s) \rightarrow CO_2 + Rh(s)$ (RS-11)

For each adsorbed species, the thermodynamic data used in evaluation of thermodynamic properties (entropy, enthalpy, heat capacity) and reverse reaction rate constants are adopted from Deutschmann's work [30,32–34].

For this study, the model is limited to a partial plasma-catalytic coupling, i.e. only few gaseous species are subject to adsorption/desorption like the reactants (CO_2, CH_4) and few intermediates/products (CO, H_2, O_2 and H_2O). The surface mechanism adopted in the model only considers the following adsorbed intermediates: H(s), OH(s), C(s), CH_3(s), CH_2(s), CH(s), O(s) and COOH(s), while more complex intermediates are created and remain in the gas phase. This limitation is mainly attributed to a lack of kinetic data but also to a poor knowledge on the plasma-catalytic interactions. The current model is a starting point and will progressively be improved as new experimental insights are obtained.

3. Results and discussion

3.1 Power deposition and electron temperature

We apply one plasma pulse which is simplified based on the voltage and current measured from our plasma reactor (Fig. S1). In our modelling, the power is input during a pulse duration of 60 ns then stopped during an afterglow period of 0.001 s (shown in Fig. 2a). A triangular pulse with a maximum power deposition of 3.0×10^5 Watts is applied to simulate the input power in one cycle [13]. Other calculation parameters are listed in Table S3. The electron temperature dose not exhibit a similar triangular pulse because the heating rate of electrons in strong electric field is nonlinear. The electron temperature gradually increases in the plasma pulse and sharply decreases as soon as the input energy ends. For typical simulation, the maximum electron temperature could reach up to 3-4 eV. This value corresponds with that in experimental and numerical studies. Due to the delay of energy transformation to the electrons, molecules, radicals and other particles, the behavior of plasma-catalysis in our modelling is complicated which will be discussed in the following sections. Although only a single power pulse is simulated in current work, it is the foundation to investigated the cumulative effects for the future study.

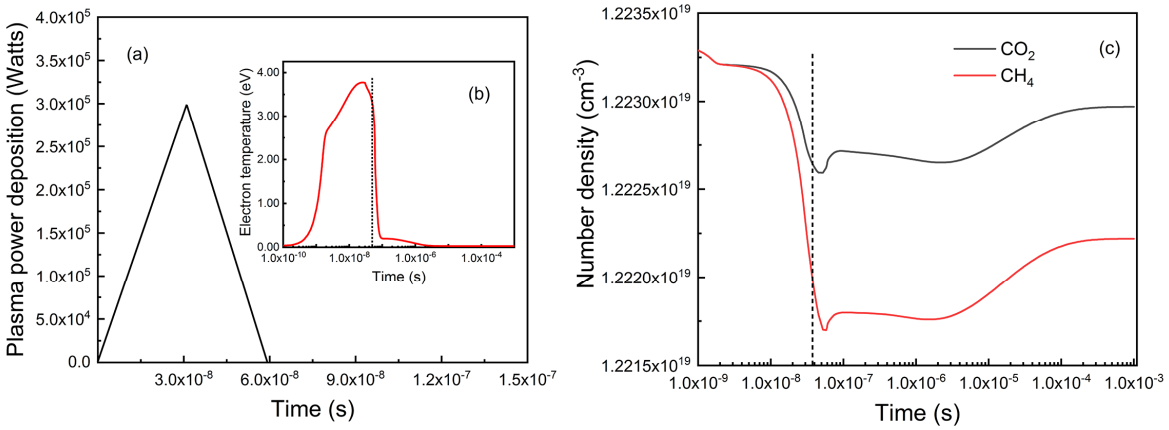

Fig. 2. (a) Plasma power deposition as a function of time $Q_{sou}(t)$, (b) electron temperature and (c) number density of reactants in one plasma pulse (before the dashed line) and afterglow (after the dashed line).

3.2 Conversion of CO_2 and CH_4

Before all else, the number density of CO_2 and CH_4 are simulated and shown in Fig. 2c. The dissociation of CO_2 and CH_4 both undergo a delay, which could be attributed to the gradually increasing electron temperature, since the initiation of the plasma. In the first 1.0×10^{-10} s of plasma initiation, the electron temperature gradually increases but is below 1 eV, which is not enough to rapidly dissociate the reactants. At 1.5×10^{-08} s, the electron temperature reaches the maximum, at this time the reaction speed of each element increases and their dissociation accelerates. At this stage, the main reaction type involved in the reaction is electron involved reactions. Interestingly, when the plasma stops, they rise first, which may be caused by the sudden drop in electron temperature. The decrease in electron temperature leads to a substantial decrease in the rate of CO_2 and CH_4 dissociation with electron participation. Then neutral reactions involving free radicals dominate, resulting in a slight decrease in the number density of reactants. Finally, due to the recombination reaction of many free radicals (CH_3, H, CO, OH and etc.,), CO_2 and CH_4 are produced, and their number density increases and tends to be balance. Overall, the conversion of carbon dioxide is slightly lower than that of methane, which is consistent with the experimental data. The detailed generation and consumption channels of CO_2 and CH_4 at each stage will be described in the next section.

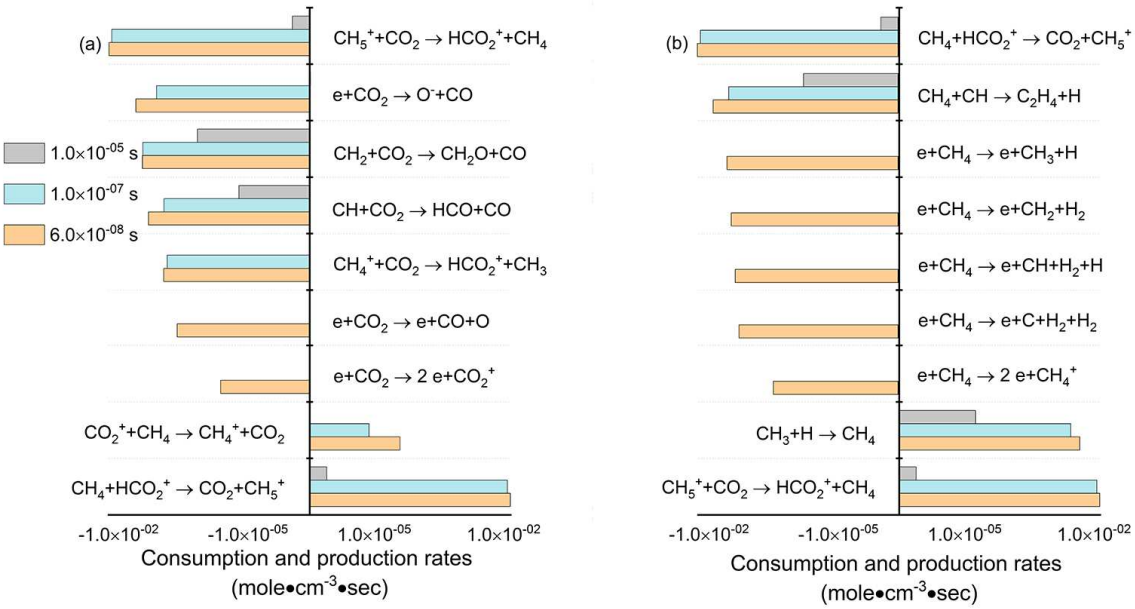

Fig. 3. Consumption (left-side of the figures) and production (right-side of the figures) rates of critical reaction channels for the production of (a) CO_2, (b) CH_4 at 6.0×10^{-08} s, 1.0×10^{-07} s and 1.0×10^{-05} s.

To better understand the micro process, as illustrated in Fig. 3, three critical stages in our model, including the plasma power deposition (6.0×10^{-08} s), termination of the power deposition (1.0×10^{-07} s) and the afterglow (1.0×10^{-05} s), are analyzed by comparing the production (consumption: for the reactants) rate of selected 10 key elementary reactions for each compound. At the beginning of the discharge, the electron temperature and density start to increase and this indicate that the electron impacted reactions occupy the decomposition pathway of the reactants. For CH_4, it is noted that CH_4 is activated via ionization (e.g. R-001) and electron impacted dissociation (e.g. R-002 and R-003). The derivative products would be further consumed (e.g. R-009 and R-037) when collide with another energetic electrons.

$$e + CH_4 \rightarrow 2e + CH_4^+ \qquad \text{(R-001)}$$

$$e + CH_4 \rightarrow e + CH_3 + H \qquad \text{(R-002)}$$

$$e + CH_4 \rightarrow e + CH_2 + H_2 \qquad \text{(R-003)}$$

$e + CH_3 \rightarrow 2e + CH_3^+$ (R-009)

$e + CH_4^+ \rightarrow CH_3 + H$ (R-037)

$e + CH_3^+ \rightarrow CH_2 + H$ (R-040)

For CO_2, similar reaction pathway at the early stage of the plasma are found to be:

$e + CO_2 \rightarrow 2e + CO_2^+$ (R-023)

$e + CO_2 \rightarrow e + CO + O$ (R-025)

$e + CO_2^+ \rightarrow CO + O$ (R-072)

Besides, the neutral radicals, oxygenates and cationic also participate in the conversion of CO_2 and CH_4:

$CH_4 + CH \rightarrow C_2H_4 + H$ (R-083)

$CH_2 + CO_2 \rightarrow CH_2O + CO$ (R-212)

$CH + CO_2 \rightarrow HCO + CO$ (R-225)

$CO_2^+ + CH_4 \rightarrow CH_4^+ + CO_2$ (R-600)

$CH_4 + HCO_2^+ \rightarrow CO_2 + CH_5^+$ (R-813)

$CH_4^+ + CO_2 \rightarrow HCO_2^+ + CH_3$ (R-818)

$CH_5^+ + CO_2 \rightarrow HCO_2^+ + CH_4$ (R-820)

After the termination of the discharge, the neutral-neutral reactions and the ion-neutral reactions gradually dominate due to the short life time of electrons and the aggregation of derivative intermediates. CO_2 is activated and decomposed in the form of collision with free radicals or positive ions (e.g. R-212, R-225, R-818 and etc.), while CH_4 also could be dissociated and form hydrocarbons through those routes (e.g. R-083, R-813, R-818 and etc.). Those reactions cause the formation of more intermediates, but at 1.0×10^{-05} s, only neutral-neutral reactions are observed to

exist in the simulated plasma process due to the decreased number density of ions. This suggests that ions species are converted back to the neutral species.

3.3 Production of C_2 hydrocarbons

As reported in our previous work, C_2 hydrocarbons, especially unsaturated hydrocarbons, are high value-added products in chemical industry. Hence, the time evolutions of C_2 hydrocarbons (C_2H_6, C_2H_4 and C_2H_2) and number density are simulated and compared in Fig. 4. We notice that in the plasma pulse, the rate of C_2H_4 formation is the fastest, and it is the dominant product of C_2 hydrocarbons in the plasma environment. However, after the power deposition, the number density of C_2H_4 decreases slightly around 1.0×10^{-05} s due to hydrogenation reaction, while the number density of C_2H_6 keeps increasing. In the C_2 hydrocarbons, saturated C_2H_6 is the main product while the selectivity of unsaturated hydrocarbons with higher value decreases. It is worth noting that the ratio of unsaturated hydrocarbon to saturated hydrocarbon (U/S ratio) would gradually decrease in afterglow and finally reach 0.31606 in our modelling.

As shown in Fig. 4c, it clearly indicates that time delay does exist between different species. First, the total production rates of C_2H_4, C_2H_6 and C_2H_2 increase in succession, then, their production terminate in the afterglow. Exceptionally, an extra peak of C_2H_6 production rate draws our attention which might indicate that C_2H_6 is formed via some neutral reaction channels during the afterglow. Between those two peaks, C_2H_5 production rate is found to exhibit a broad peak (1.0×10^{-07} s) spanning the plasma pulse and afterglow. The possible explanation is that part of C_2H_4 is consumed via the hydrogenation and recombination which contribute to the formation of C_2H_5 specie and higher hydrocarbons (Fig. 5a) [8]. Subsequently, as shown in Fig. 5b and 4c, C_2H_5 specie will be further reduced to C_2H_6 which is corresponding to the production peak in the afterglow. The processes ($C_2H_4 \rightarrow C_2H_5 \rightarrow C_2H_6$) restrict the selectivity of unsaturated hydrocarbons, hence, some approaches, including the design of special catalysts, optimization of plasma input, could be investigated to achieve higher selectivity of unsaturated hydrocarbons by inhibiting the process mentioned.

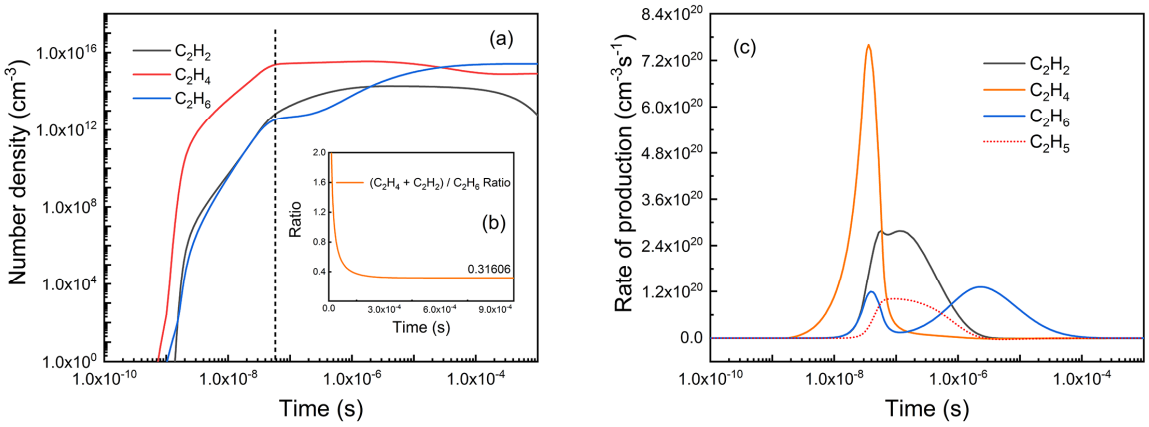

Fig. 4. (a) Number density, (b) U/S ratio and (c) production rates of C_2 hydrocarbons as a function of time.

To investigate the insight of hydrocarbons formation, we subsequently analyze the detailed reaction progress of C_2H_4, C_2H_5 and C_2H_6 at different stages. The main reaction channels differ significantly in terms of time scale. In the plasma pulse, the combination between the derivative radicals not only dominates the formation reaction of C_2H_4 but also contribute to the formation of C_2H_6 (e.g. R-090, R-091, R-092 and etc.) [35].

$$CH_3 + CH_3 \rightarrow C_2H_6 \qquad \text{(R-090)}$$

$$CH_3 + CH_3 \rightarrow C_2H_4 + H_2 \qquad \text{(R-091)}$$

$$CH_3 + CH_2 \rightarrow C_2H_4 + H \qquad \text{(R-092)}$$

After the power pulse, parts of those reaction rates are significantly reduced while others become more dominant (Fig. 5). For instance, the reactions involving C_2H_4, the C_2H_4 hydrogenation becomes the dominant reaction at 1.0×10^{-05} s and consequently a large amount of C_2H_5 radicals are produced in this duration. The crucial product, C_2H_4, are converted via neutral reactions (e.g. R-109, R-132 and etc.) rather than electron reactions (e.g. R-018 and etc.). This indicates that concentration of unsaturated hydrocarbons would shift to the chemical equilibrium instantly out of the plasma environment. Amount them, the H attachment to C_2H_4 occupy the main route.

$$e + C_2H_4 \rightarrow e + C_2H_3 + H \qquad \text{(R-018)}$$

$CH_2 + C_2H_4 \rightarrow C_3H_6$ (R-109)

$C_2H_4 + H \rightarrow C_2H_5$ (R-132)

Correspondingly, C_2H_5 further hydrogenation (e.g. R-127, R-128, R-130 and etc.) gradually becomes a major reaction path for the formation of C_2H_6 after the end of pulse and finally occupies a dominant position in the afterglow.

$C_2H_5 + CH_4 \rightarrow C_2H_6 + CH_3$ (R-084)

$C_2H_5 + H_2 \rightarrow C_2H_6 + H$ (R-127)

$C_2H_5 + H \rightarrow CH_3 + CH_3$ (R-128)

$C_2H_5 + H \rightarrow C_2H_6$ (R-130)

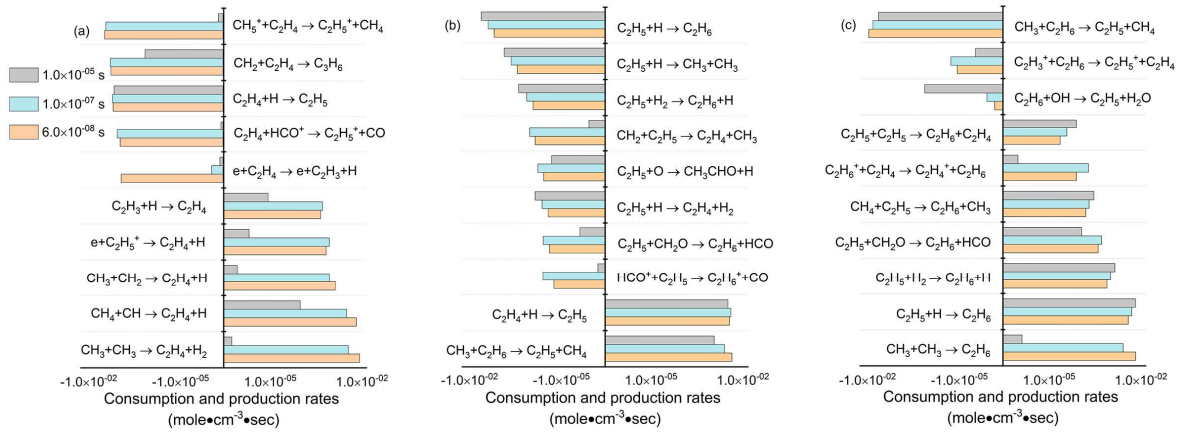

Fig. 5. Consumption (left-side of the figures) and production (right-side of the figures) rates of critical reaction channels for the production of (a) C_2H_4, (b) C_2H_5 and (c) C_2H_6 at 6.0×10^{-08} s, 1.0×10^{-07} s and 1.0×10^{-05} s.

In thermal-catalysis, several mechanisms, involving a RWGS step and Fischer–Tropsch synthesis (FTS) step, were proposed for the hydrocarbon formation [36]. The carbide mechanism via FTS is the most plausible one. Monomer species, methylene (CH2), are formed on the surface and then followed by chain propagation in which other monomers are inserted into a growing alkyl chain.

We believe that more comprehensive understanding of surface mechanisms on plasma-catalyst would be attractive.

3.4 Reaction barrier and surface mechanism

The apparent activation energy is often used to evaluate the energetic threshold for reactions. It enables us to deal with the reaction process from the fundamental microscopic nature of chemical collisions to macroscopic aspects of chemical reactions. Hence, the in-depth understanding of the plasma-catalyst's effect on activation energy is crucial, so, we discuss this vital kinetic parameter in this section. Table S3 shows the critical input information and values for the calculation of apparent activation energy. According to the modified Arrhenius equation introduced in section 2., the flow rate and power deposition are set as 50 mL/min and 2-3 W respectively while the other parameters remain the same value. Typically, two surface mechanisms on the Ni based catalysts are evaluated so that we could investigate the effects of catalysts in plasma surroundings. Dry reforming over Rh based catalyst is also studied especially.

The apparent activation energy of the plasma assisted dry reforming without catalyst and over Rh-based catalyst are compared in Fig. 6. The plasma process exhibits a typical Arrhenius behavior and the apparent activation energy of CO_2 and CH_4 are estimated to be 55.41 kJ mol^{-1} and 58.65 kJ mol^{-1}. It is critical to mention that the apparent activation energy decreases after introducing the surface reactions on the Rh sites. The apparent activation energy of CO_2 and CH_4 decrease to 42.97 kJ mol^{-1} and 48.65 kJ mol^{-1} respectively due to the interactions of plasma and catalysts. Compared with plasma process, the apparent activation energy decreases up to 22.45% and 16.90% respectively. The catalysts provide an alternative route in which less activation energy (Fig. 6) is required. The adsorbed species, such as $CO_2(s)$ and $CH_4(s)$, are activated by other species stick on Rh sites [30]:

$CO_2(s) + H(s) \rightarrow COOH(s)$ (RS-26)

$CO_2(s) + H(s) \rightarrow CO(s) + OH(s)$ (RS-30)

$CH_4(s) + O(s) \rightarrow CH_3(s) + OH(s)$ (RS-41)

As a result, new transition species and states, such as COOH(s), CH_3(s) and etc., are produced via this novel approach which require less energy. Chain decompositions of CH_4 exist and produce adsorbed intermediates:

$CH_3(s) + Rh(s) \rightarrow CH_2(s) + H(s)$ (RS-35)

$CH_2(s) + Rh(s) \rightarrow CH(s) + H(s)$ (RS-37)

We also notice that, besides the direct dissociation of CO_2(s), combination of CO_2(s) and H(s) also is significant while formed COOH(s) will further decompose.

$COOH(s) + Rh(s) \rightarrow CO(s) + OH(s)$ (RS-24)

$COOH(s) + H(s) \rightarrow CO(s) + H_2O(s)$ (RS-27)

This species could further participate in the formation of organic acid, which is not described in our kinetic model, under certain conditions.

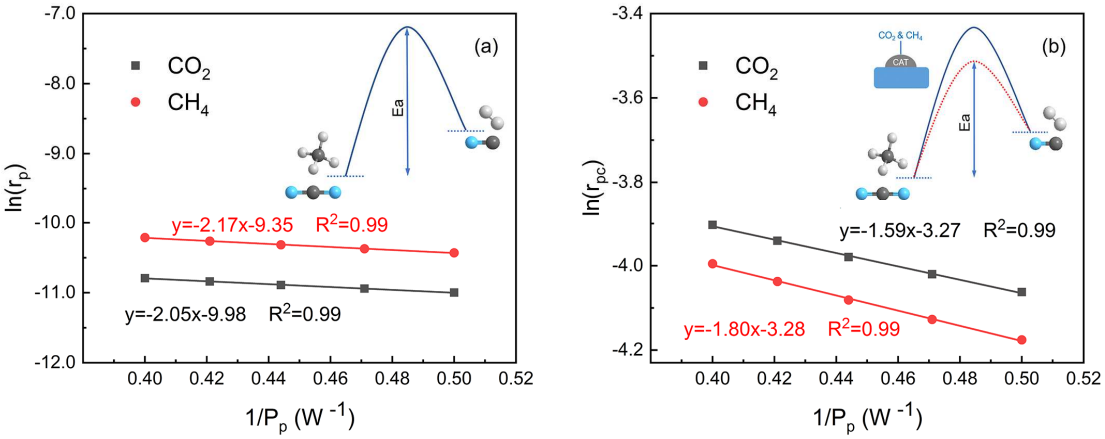

Fig. 6. The Arrhenius plot for the plasma assisted dry reforming (a) without catalyst and (b) over Rh-based catalyst.

In dry reforming, the CH_4 chemisorption (RS-06) is considered to be a rate determining step [37]. It is reported that the apparent activation energy would decrease from 91 kJ mol^{-1} to 44.7 kJ mol^{-1} (in 100 kHz DBD) due to the state-specific reactivity of vibrationally excited CH_4. In plasma assisted CH_4 reforming, vibrationally excited CH_4 in streamers contribute a lot to the enhancement

of CH_4 chemisorption which is considered to be the rate-determining step [37]. RS-06 and RS-33 cooperatively simulate such a dissociative chemisorption of CH_4 ($CH_4 \rightarrow CH_3* + H*$), which is corresponding to the increase of efficiency. Besides, the rate of adsorption, desorption, surface diffusion processes and elementary reactions on different surfaces also affects the apparent activation energy.

Comparing different surface mechanisms on Rh and Ni sites in this study, it is worthy to mention that the parameters in the Arrhenius equations for CO_2 and CH_4 adsorption processes (RS-06 and RS-04) show great difference which further affects the reaction progress. The sensitivity analysis of methane dry reforming shows that methane adsorption (RS-06) and desorption (RS-12) reactions are the most sensitive reactions [32].

There is another discussion exists in thermal-catalytic modelling. Eley-Rideal reactions play an important role in products formation. Nakamura et al., [38] reported that H_2O reacts with adsorbed CH_2 species and forms adsorbed CO and H_2 through R_{ER}-01. On the other side, gas phase CO_2 could also collide with an adsorbed H and form CO and adsorbed OH species (R_{ER}-02) [39]. Mark and Maier further proposed an alternative path for the formation of CO in which gas phase CO_2 reacts with surface carbon species (R_{ER}-03) [40]. With the help of fundamental study of surface reactions (to obtain relevant kinetic data), we will understand those Eley-Rideal reactions more globally in the future modelling of plasma-catalysis.

$CH_2(s) + H_2O \rightarrow CO(s) + 2H_2$ (R_{ER}-01)

$CO_2 + H(s) \rightarrow CO + OH(s)$ (R_{ER}-02)

$C(s) + CO_2 \rightarrow 2CO + Rh(s)$ (R_{ER}-03)

The apparent activation energy over other catalysts are summarized in Table 2. For all the simulations (simulation details are shown in Table S3) in this work, the data well fit in the Arrhenius law linearly and the R-squared (R^2) are all higher than 0.99 which indicate a goodness-of-fit. In our simulations, the apparent activation energy of CO_2 and CH_4 without catalyst, with Ni catalyst according to two different surface mechanisms adopted from works of Delgado [32] and Janardhanan [33] respectively, and with Rh catalyst according to a surface mechanism adopted from Karakaya's work [30], are compared. The catalysts clearly show capability to decrease the

apparent activation energy. The Ni-based catalysts have a comparable slope, in other word comparable reaction barrier, since they share a similar reaction route, while Rh-based catalyst exhibits even lower apparent activation energy due to their surface reactions. It is critical to mention that, for all the simulations, the apparent activation energy of the CO_2 is lower than that of CH_4. This tendency could not only be attributed to the surface properties of the metal sites but also to the reverse water gas shift (RWGS) reaction. This phenomenon is consistent with the literature [41–43]. Ladavos et al., [43] reported that, rather than just adsorb on the surface, CO_2 could react with catalyst structural phase (La_2O_3 and SrO) and form new lanthanum or strontium containing crystal phases ($La_2O_2CO_3$ and $SrCO_3$) which are characterized by XRD. Due to the strong affinity of CO_2 with the oxides and special surface destruction, the value of apparent activation energy of CO_2 consumption is lower than that of CH_4. As mentioned in the introduction and literature, lack of kinetic data for surface reactions considerably restricts the development of a more realistic model. On the other side, CO_2 is able to participate in multiple reaction pathway including RWGS ($CO_2 + H_2 \rightarrow CO + H_2O$) which is also attribute to the decreasing of its apparent activation energy [41].

Table 2. Summary of calculated apparent activation energy of CO_2 and CH_4.

INFORMATION	Plasma alone	**Ni** Plasma-catalysis according to mechanism of [33]	**Ni** Plasma-catalysis according to mechanism of [32]	**Rh** Plasma-catalysis according to mechanism of [30]
Slope (CO_2)	-2.05	-1.81	-1.83	-1.59
$R_{(CO2)}^2$	0.99	0.99	0.99	0.99
Slope (CH_4)	-2.17	-2.15	-2.04	-1.80
$R_{(CH4)}^2$	0.99	0.99	0.99	0.99
E_a (CO_2) kJ mol^{-1}	55.41	48.92	49.46	42.97
E_a (CH_4) kJ mol^{-1}	58.65	58.10	55.13	48.65

It is essential to compare our simulated values of apparent activation energy with experimental values reported in previous work. Table 3 shows the activation barrier of CO_2 and CH_4 conversion in thermal catalysis and plasma-catalysis. For the thermal catalysis, the apparent activation energies of CO_2 are reported to be 62.2 kJ mol^{-1} - 108.9 kJ mol^{-1} while it requires 65.5 kJ mol^{-1} - 87.8 kJ mol^{-1} for CH_4 activation [42,44]. The reaction barriers decrease remarkably in plasma assisted process. The apparent activation energies are estimated to be 6.1 kJ mol^{-1} - 29.5 kJ mol^{-1} and 32.6 kJ mol^{-1} - 35.2 kJ mol^{-1} for CO_2 and CH_4 respectively [24,45]. In most of works, the apparent activation energy of CO_2 is lower than CH_4 which is in line with our numerical study. Besides dry reforming, the apparent activation energy of CO_2 also declines sharply in CO_2 plasma assisted hydrogenation (21 kJ mol^{-1} - 43 kJ mol^{-1}) when it is compared with the value in thermal catalysis (68 kJ mol^{-1} - 112 kJ mol^{-1}) [29].

Table 3. Comparison of reaction barrier of reactants over different catalysts.

Catalysts	Reaction system	Reaction type	E_a (CO_2) kJ mol^{-1}	E_a (CH_4) kJ mol^{-1}	Ref
Ni/TiO_2 (673–823 K)	Thermal-catalysis	dry reforming	108.9	87.8	[42]
Ni-CeMgAl (773–873 K)	Thermal-catalysis	dry reforming	62.2	65.5	[44]
Ni/Al_2O_3 (673–783 K)	Thermal-catalysis	dry reforming	69.0	70.6	[46]
Rh/Al_2O_3 (673–783 K)	Thermal-catalysis	dry reforming	82.3	65.6	[46]
Rh/SiO_2 (673–783 K)	Thermal-catalysis	dry reforming	54.8	74.8	[46]
Ni-SiO_2	Plasma-catalysis	dry reforming	-	6.1-18.6	[24]
Ni/La_2O_3-$MgAl_2O_4$	Plasma-catalysis	dry reforming	35.2	32.6	[45]
Ni–La_2O_3@SiO_2	Plasma-catalysis	dry reforming	29.5	24.7	[47]
Ni-based	Plasma-catalysis	dry reforming	49.46	55.13	This work
Rh-based	Plasma-catalysis	dry reforming	42.97	48.65	This work

For modelling a combustion and/or thermal-catalytic process in a CFD solver, the corresponding reaction mechanism is commonly implemented in the thermofluidic model which composes the basis of the solver [48–50]. Such a numerical model could not only indicate spatial-temporal distributions of major species but also describe the effects of turbulence, reactor geometry, etc. on the process. Hence, we expect that the chemical model built in this work can be adopted for higher dimensional modelling of plasma-catalysis by implementation in a CFD solver, like FLUENT, to have a better idea of the chemical dynamics, and not only the kinetics, in our configurations of reactor and flowing.

4. Conclusion

In this numerical work, we investigated the kinetic aspect of plasma-catalytic dry reforming via a zero-dimension plasma-catalytic model in a batch reactor. A kinetic method for evaluating the role of the electrons and the catalyst in this plasma-catalysis process is proposed. The number densities of reactants, products and key intermediates were calculated during one plasma pulse. For C_2 hydrocarbons, in agreement with previous published experimental results [3], C_2H_6 was found to be the main product. The ratio of unsaturated over saturated hydrocarbons first increases and then decreases in the plasma pulse, and finally returns to an equilibrium value. This could explain the limitation of this ratio observed in the experimental studies. It may be related to two successive processes: a dehydrogenation during the plasma phase followed by a re-hydrogenation after plasma extinction. In this frame, we observed that C_2H_5, an intermediate, plays an important role in the plasma-catalytic reduction of C_2H_4 to C_2H_6. The detailed reaction pathway was investigated via time scale analysis of reaction rates of important elementary reactions. The apparent activation barriers of plasma assisted dry reforming with or without catalysts are calculated and fitted by a modified Arrhenius law which are rarely calculated by computational method in previous study. In this study, by inducing reported surface mechanisms over Rh and Ni catalysts, it was shown that the apparent activation energies decreased by 22.45% and 17.05% for CO_2 conversion and CH_4 conversion respectively. These results show by a numerical way the advantage in terms of energy of plasma-catalytic conversion face of nonthermal plasma conversion alone. However, this first complete study is based on several approximations to simplify the model. The main one is the consideration of a partial plasma-catalytic coupling due to the lack of experimental data. In future, the model will be extended to a full plasma-catalytic coupling supported by new experimental data

in order to get closer to the reality. Other crucial factors such as accumulation effect of charges and species should not be ignored either.

Acknowledgements

This work was supported by Mines Paris, Université PSL and Institut Mines-Télécom. Shengfei Wang thanks them for their support to his PhD scholarship.

References

[1] E.C. Neyts, K. (Ken) Ostrikov, M.K. Sunkara, A. Bogaerts, Plasma Catalysis: Synergistic Effects at the Nanoscale, Chem. Rev. 115 (2015) 13408–13446. https://doi.org/10.1021/acs.chemrev.5b00362.

[2] E.C. Neyts, A. Bogaerts, Understanding plasma catalysis through modelling and simulation—a review, J. Phys. D: Appl. Phys. 47 (2014) 224010. https://doi.org/10.1088/0022-3727/47/22/224010.

[3] D. Li, V. Rohani, F. Fabry, A. Parakkulam Ramaswamy, M. Sennour, L. Fulcheri, Direct conversion of CO2 and CH4 into liquid chemicals by plasma-catalysis, Applied Catalysis B: Environmental. 261 (2020) 118228. https://doi.org/10.1016/j.apcatb.2019.118228.

[4] L. Wang, Y. Yi, C. Wu, H. Guo, X. Tu, One-Step Reforming of CO2 and CH4 into High-Value Liquid Chemicals and Fuels at Room Temperature by Plasma-Driven Catalysis, Angewandte Chemie International Edition. 56 (2017) 13679–13683. https://doi.org/10.1002/anie.201707131.

[5] S. Xu, S. Chansai, C. Stere, B. Inceesungvorn, A. Goguet, K. Wangkawong, S.F.R. Taylor, N. Al-Janabi, C. Hardacre, P.A. Martin, X. Fan, Sustaining metal–organic frameworks for water–gas shift catalysis by non-thermal plasma, Nat Catal. 2 (2019) 142–148. https://doi.org/10.1038/s41929-018-0206-2.

[6] M. Mikhail, B. Wang, R. Jalain, S. Cavadias, M. Tatoulian, S. Ognier, M.E. Gálvez, P. Da Costa, Plasma-catalytic hybrid process for CO2 methanation: optimization of operation parameters, Reac Kinet Mech Cat. 126 (2019) 629–643. https://doi.org/10.1007/s11144-018-1508-8.

[7] C.E. Stere, W. Adress, R. Burch, S. Chansai, A. Goguet, W.G. Graham, C. Hardacre, Probing a Non-Thermal Plasma Activated Heterogeneously Catalyzed Reaction Using in Situ DRIFTS-MS, ACS Catal. 5 (2015) 956–964. https://doi.org/10.1021/cs5019265.

[8] A. Bogaerts, C. De Bie, R. Snoeckx, T. Kozák, Plasma based CO2 and CH4 conversion: A modeling perspective, Plasma Processes and Polymers. 14 (2017) 1600070. https://doi.org/10.1002/ppap.201600070.

[9] C. De Bie, J. van Dijk, A. Bogaerts, The Dominant Pathways for the Conversion of Methane into Oxygenates and Syngas in an Atmospheric Pressure Dielectric Barrier Discharge, J. Phys. Chem. C. 119 (2015) 22331–22350. https://doi.org/10.1021/acs.jpcc.5b06515.
[10] S. Heijkers, L.M. Martini, G. Dilecce, P. Tosi, A. Bogaerts, Nanosecond Pulsed Discharge for CO_2 Conversion: Kinetic Modeling To Elucidate the Chemistry and Improve the Performance, J. Phys. Chem. C. 123 (2019) 12104–12116. https://doi.org/10.1021/acs.jpcc.9b01543.
[11] R. Snoeckx, R. Aerts, X. Tu, A. Bogaerts, Plasma-Based Dry Reforming: A Computational Study Ranging from the Nanoseconds to Seconds Time Scale, J. Phys. Chem. C. 117 (2013) 4957–4970. https://doi.org/10.1021/jp311912b.
[12] K. Van Laer, A. Bogaerts, Influence of Gap Size and Dielectric Constant of the Packing Material on the Plasma Behaviour in a Packed Bed DBD Reactor: A Fluid Modelling Study: Influence of Gap Size and Dielectric Constant…, Plasma Process Polym. 14 (2017) 1600129. https://doi.org/10.1002/ppap.201600129.
[13] R. Aerts, T. Martens, A. Bogaerts, Influence of Vibrational States on CO_2 Splitting by Dielectric Barrier Discharges, J. Phys. Chem. C. 116 (2012) 23257–23273. https://doi.org/10.1021/jp307525t.
[14] J. Hong, S. Pancheshnyi, E. Tam, J.J. Lowke, S. Prawer, A.B. Murphy, Kinetic modelling of NH3 production in N2–H2 non-equilibrium atmospheric-pressure plasma catalysis, J. Phys. D: Appl. Phys. 50 (2017) 154005. https://doi.org/10.1088/1361-6463/aa6229.
[15] Y. Engelmann, K. van 't Veer, Y. Gorbanev, E.C. Neyts, W.F. Schneider, A. Bogaerts, Plasma Catalysis for Ammonia Synthesis: A Microkinetic Modeling Study on the Contributions of Eley–Rideal Reactions, ACS Sustainable Chem. Eng. 9 (2021) 13151–13163. https://doi.org/10.1021/acssuschemeng.1c02713.
[16] H. Ma, W.F. Schneider, Plasma-catalyst modeling for materials selection: challenges and opportunities in nitrogen oxidation, J. Phys. D: Appl. Phys. 54 (2021) 454004. https://doi.org/10.1088/1361-6463/ac1bd1.
[17] P. Mehta, P. Barboun, F.A. Herrera, J. Kim, P. Rumbach, D.B. Go, J.C. Hicks, W.F. Schneider, Overcoming ammonia synthesis scaling relations with plasma-enabled catalysis, Nat Catal. 1 (2018) 269–275. https://doi.org/10.1038/s41929-018-0045-1.
[18] P.-A. Maitre, M.S. Bieniek, P.N. Kechagiopoulos, Plasma-Catalysis of Nonoxidative Methane Coupling: A Dynamic Investigation of Plasma and Surface Microkinetics over Ni(111), J. Phys. Chem. C. 126 (2022) 19987–20003. https://doi.org/10.1021/acs.jpcc.2c03503.
[19] Y. Engelmann, P. Mehta, E.C. Neyts, W.F. Schneider, A. Bogaerts, Predicted Influence of Plasma Activation on Nonoxidative Coupling of Methane on Transition Metal Catalysts, ACS Sustainable Chem. Eng. 8 (2020) 6043–6054. https://doi.org/10.1021/acssuschemeng.0c00906.
[20] N. Pourali, M. Vasilev, R. Abiev, E.V. Rebrov, Development of a microkinetic model for non-oxidative coupling of methane over a Cu catalyst in a non-thermal plasma reactor, J. Phys. D: Appl. Phys. 55 (2022) 395204. https://doi.org/10.1088/1361-6463/ac7fc6.
[21] B. Loenders, Y. Engelmann, A. Bogaerts, Plasma-Catalytic Partial Oxidation of Methane on Pt(111): A Microkinetic Study on the Role of Different Plasma Species, J. Phys. Chem. C. 125 (2021) 2966–2983. https://doi.org/10.1021/acs.jpcc.0c09849.

[22] R. Michiels, Y. Engelmann, A. Bogaerts, Plasma Catalysis for CO2 Hydrogenation: Unlocking New Pathways toward CH3OH, J. Phys. Chem. C. 124 (2020) 25859–25872. https://doi.org/10.1021/acs.jpcc.0c07632.
[23] J. Du, L. Zong, S. Zhang, Y. Gao, L. Dou, J. Pan, T. Shao, Numerical investigation on the heterogeneous pulsed dielectric barrier discharge plasma catalysis for CO2 hydrogenation at atmospheric pressure: Effects of Ni and Cu catalysts on the selectivity conversions to CH4 and CH3OH, Plasma Processes and Polymers. 19 (2022) 2100111. https://doi.org/10.1002/ppap.202100111.
[24] J. Kim, D.B. Go, J.C. Hicks, Synergistic effects of plasma–catalyst interactions for CH4 activation, Phys. Chem. Chem. Phys. 19 (2017) 13010–13021. https://doi.org/10.1039/C7CP01322A.
[25] H. Zheng, Q. Liu, Kinetic Study of Nonequilibrium Plasma-Assisted Methane Steam Reforming, Mathematical Problems in Engineering. 2014 (2014) 1–10. https://doi.org/10.1155/2014/938618.
[26] L.M. Martini, G. Dilecce, G. Guella, A. Maranzana, G. Tonachini, P. Tosi, Oxidation of CH4 by CO2 in a dielectric barrier discharge, Chemical Physics Letters. 593 (2014) 55–60. https://doi.org/10.1016/j.cplett.2013.12.069.
[27] J.A. Manion, R.E. Huie, R.D. Levin, D.R. Burgess Jr., V.L. Orkin, W. Tsang, W.S. McGivern, J.W. Hudgens, V.D. Knyazev, D.B. Atkinson, E. Chai, A.M. Tereza, C.Y. Lin, T.C. Allison, W.G. Mallard, F. Westley, J.T. Herron, R.F. Hampson, D.H. Frizzell, NIST Chemical Kinetics Database, NIST Chemical Kinetics Database, NIST Standard Reference Database 17, Version 7.0 (Web Version), Release 1.6.8, Data Version 2015.09, National Institute of Standards and Technology, Gaithersburg, Maryland, 20899-8320. (n.d.).
[28] D. McElroy, C. Walsh, A.J. Markwick, M.A. Cordiner, K. Smith, T.J. Millar, The UMIST database for astrochemistry 2012, A&A. 550 (2013) A36. https://doi.org/10.1051/0004-6361/201220465.
[29] S. Xu, S. Chansai, Y. Shao, S. Xu, Y. Wang, S. Haigh, Y. Mu, Y. Jiao, C.E. Stere, H. Chen, X. Fan, C. Hardacre, Mechanistic study of non-thermal plasma assisted CO2 hydrogenation over Ru supported on MgAl layered double hydroxide, Applied Catalysis B: Environmental. 268 (2020) 118752. https://doi.org/10.1016/j.apcatb.2020.118752.
[30] C. Karakaya, L. Maier, O. Deutschmann, Surface Reaction Kinetics of the Oxidation and Reforming of CH4 over Rh/Al2O3 Catalysts, International Journal of Chemical Kinetics. 48 (2016) 144–160. https://doi.org/10.1002/kin.20980.
[31] Z. Xie, Q. Liao, M. Liu, Z. Yang, L. Zhang, Micro-kinetic modeling study of dry reforming of methane over the Ni-based catalyst, Energy Conversion and Management. 153 (2017) 526–537. https://doi.org/10.1016/j.enconman.2017.10.022.
[32] K. Delgado, L. Maier, S. Tischer, A. Zellner, H. Stotz, O. Deutschmann, Surface Reaction Kinetics of Steam- and CO2-Reforming as Well as Oxidation of Methane over Nickel-Based Catalysts, Catalysts. 5 (2015) 871–904. https://doi.org/10.3390/catal5020871.
[33] V.M. Janardhanan, O. Deutschmann, CFD analysis of a solid oxide fuel cell with internal reforming: Coupled interactions of transport, heterogeneous catalysis and electrochemical processes, Journal of Power Sources. 162 (2006) 1192–1202. https://doi.org/10.1016/j.jpowsour.2006.08.017.
[34] L. Maier, B. Schädel, K. Herrera Delgado, S. Tischer, O. Deutschmann, Steam Reforming of Methane Over Nickel: Development of a Multi-Step Surface Reaction Mechanism, Top Catal. 54 (2011) 845–858. https://doi.org/10.1007/s11244-011-9702-1.

[35] C. De Bie, B. Verheyde, T. Martens, J. van Dijk, S. Paulussen, A. Bogaerts, Fluid Modeling of the Conversion of Methane into Higher Hydrocarbons in an Atmospheric Pressure Dielectric Barrier Discharge: Fluid Modeling of the Conversion of Methane …, Plasma Processes Polym. 8 (2011) 1033–1058. https://doi.org/10.1002/ppap.201100027.
[36] M. Ronda-Lloret, G. Rothenberg, N.R. Shiju, A Critical Look at Direct Catalytic Hydrogenation of Carbon Dioxide to Olefins, ChemSusChem. 12 (2019) 3896–3914. https://doi.org/10.1002/cssc.201900915.
[37] Z. Sheng, Y. Watanabe, H.-H. Kim, S. Yao, T. Nozaki, Plasma-enabled mode-selective activation of CH4 for dry reforming: First touch on the kinetic analysis, Chemical Engineering Journal. 399 (2020) 125751. https://doi.org/10.1016/j.cej.2020.125751.
[38] J. Nakamura, K. Aikawa, K. Sato, T. Uchijima, Role of support in reforming of CH4 with CO2 over Rh catalysts, Catal Lett. 25 (1994) 265–270. https://doi.org/10.1007/BF00816306.
[39] A. Erdohelyi, J. Cserenyi, F. Solymosi, Activation of CH4 and Its Reaction with CO2 over Supported Rh Catalysts, Journal of Catalysis. 141 (1993) 287–299. https://doi.org/10.1006/jcat.1993.1136.
[40] M.F. Mark, W.F. Maier, CO2-Reforming of Methane on Supported Rh and Ir Catalysts, Journal of Catalysis. 164 (1996) 122–130. https://doi.org/10.1006/jcat.1996.0368.
[41] N.H. Elsayed, N.R.M. Roberts, B. Joseph, J.N. Kuhn, Low temperature dry reforming of methane over Pt–Ni–Mg/ceria–zirconia catalysts, Applied Catalysis B: Environmental. 179 (2015) 213–219. https://doi.org/10.1016/j.apcatb.2015.05.021.
[42] J. Zhang, H. Wang, A.K. Dalai, Kinetic Studies of Carbon Dioxide Reforming of Methane over Ni−Co/Al−Mg−O Bimetallic Catalyst, Ind. Eng. Chem. Res. 48 (2009) 677–684. https://doi.org/10.1021/ie801078p.
[43] Ch. Pichas, P. Pomonis, D. Petrakis, A. Ladavos, Kinetic study of the catalytic dry reforming of CH4 with CO2 over La2−xSrxNiO4 perovskite-type oxides, Applied Catalysis A: General. 386 (2010) 116–123. https://doi.org/10.1016/j.apcata.2010.07.043.
[44] Z. Bao, Y. Lu, F. Yu, Kinetic study of methane reforming with carbon dioxide over NiCeMgAl bimodal pore catalyst, AIChE Journal. 63 (2017) 2019–2029. https://doi.org/10.1002/aic.15579.
[45] A.H. Khoja, M. Tahir, N.A.S. Amin, A. Javed, M.T. Mehran, Kinetic study of dry reforming of methane using hybrid DBD plasma reactor over La2O3 co-supported Ni/MgAl2O4 catalyst, International Journal of Hydrogen Energy. 45 (2020) 12256–12271. https://doi.org/10.1016/j.ijhydene.2020.02.200.
[46] P. Ferreira-Aparicio, A. Guerrero-Ruiz, I. Rodríguez-Ramos, Comparative study at low and medium reaction temperatures of syngas production by methane reforming with carbon dioxide over silica and alumina supported catalysts, Applied Catalysis A: General. 170 (1998) 177–187. https://doi.org/10.1016/S0926-860X(98)00048-9.
[47] X. Zheng, S. Tan, L. Dong, S. Li, H. Chen, Silica-coated LaNiO3 nanoparticles for non-thermal plasma assisted dry reforming of methane: Experimental and kinetic studies, Chemical Engineering Journal. 265 (2015) 147–156. https://doi.org/10.1016/j.cej.2014.12.035.
[48] Y. Tu, W. Yang, H. Liu, A Refined Global Reaction Mechanism for Gently Preheated MILD Combustion of Methane, Energy Fuels. 31 (2017) 10144–10157. https://doi.org/10.1021/acs.energyfuels.7b01666.

[49] J.M. Blasi, R.J. Kee, In situ adaptive tabulation (ISAT) to accelerate transient computational fluid dynamics with complex heterogeneous chemical kinetics, Computers & Chemical Engineering. 84 (2016) 36–42. https://doi.org/10.1016/j.compchemeng.2015.08.020.
[50] Z. Mansouri, Combustion in wavy micro-channels for thermo-photovoltaic applications – Part I: Effects of wavy wall geometry, wall temperature profile and reaction mechanism, Energy Conversion and Management. 198 (2019) 111155. https://doi.org/10.1016/j.enconman.2018.12.105.

Graphical Abstract